AIAA JOURNAL
Vol. 45, No. 5, May 2007

Restricted Modal Analysis Applied to Internal Annular Combustor Autospectra and Cross-Spectra Measurements

Jeffrey Hilton Miles*
NASA John H. Glenn Research Center at Lewis Field, Cleveland, Ohio 44135

DOI: 10.2514/1.25179

A treatment of the modal decomposition of the pressure field in a combustor as determined by two pressure time history measurements is developed herein. It is applied to a Pratt and Whitney PW4098 engine combustor over a range of operating conditions. For modes other than the plane wave the assumption is made that there are distinct frequency bands in which the individual modes, including the plane wave mode, overlap such that if circumferential mode m and circumferential mode $m-1$ are present then circumferential mode $m-2$ is not. In the analysis used herein at frequencies above the first cutoff mode frequency, only pairs of circumferential modes are individually present at each frequency. Consequently, this is a restricted modal analysis. As part of the analysis one specifies mode cut-on frequencies. This creates a set of frequencies that each mode spans. One finding was the successful use of the same modal span frequencies over a range of operating conditions for this particular engine. This suggests that for this case the cut-on frequencies are in proximity at each operating condition. Consequently, the combustion noise spectrum related to the circumferential modes might not change much with operating condition.

Nomenclature

A	=	amplitude of clockwise pressure wave
$a_{m\mu}^{(\sigma)}$	=	eigenvalue from Eq. (14)
B	=	amplitude of counterclockwise pressure wave
B_e	=	resolution bandwidth, Hz, $B_e = 1/T_d = r/Np = 11.71875$ Hz
c	=	speed of sound in m/s
D	=	delay time τ, s (sometimes expressed as a number of samples, $D = \tau 48000$)
$E_{m\mu}^{(\sigma)}(a_{m\mu}^{(\sigma)}\frac{r}{r_b})$	=	radial duct mode Eq. (13)
f	=	frequency, Hz
f_c	=	upper frequency limit, $f_c = 1/2\Delta t = r/2$, Hz (24,000 Hz)
f_{critical}	=	Eq. (17)
$f_{\text{cutoff}}(\bar{M}_{\text{duct}})$	=	Eq. (18)
$G_{xx}(f)$	=	power spectral density
$G_{xy}(f)$	=	cross power spectral density
J_m, Y_m	=	Bessel function of first and second kind and order m
j	=	positive imaginary square root of -1, $\sqrt{-1}$
L_c	=	cost function
L_y	=	number of frequencies, $f_c/\Delta f = Np/2$ (2048)
$\bar{M}_{\text{duct}}$	=	duct Mach number
m	=	circumferential mode order
Np	=	segment length, number of data points per segment (4096)
n_d	=	number of disjoint (independent) data segments/blocks, $n_d = B_e T_{\text{total}} = 234$
$n_{o\ell}$	=	number of overlapped segments, with 50% overlap $n_{o\ell} = 468$
n_s	=	number of segments
$P(f)$	=	Fourier transform of $p(t)$
$p(t)$	=	pressure signal
p_k	=	conversion constant, $10^{(171/20)}/0.25$
$Q_{m\mu}^{(\sigma)}$	=	eigenvalue from Eq. (15)
q_0	=	contaminating noise at station 0
q_θ	=	contaminating noise at station θ
r	=	sample rate, samples/s (48,000)
r_a	=	exterior concentric cylindrical duct radius
r_b	=	interior concentric cylindrical duct radius
s_1	=	signal at station 1
s_2	=	signal at station 2
T	=	temperature, K
$T_d(i)$	=	record length of segment i
T_{total}	=	total record length, s ($\approx$20 s)
t	=	time
w	=	weighting function also known as a window function
$Z(z)$	=	axial propagating component of the pressure Eq. (16)
z, r, ϕ	=	cylindrical coordinates
γ_{nn}^2	=	analytical coherence threshold
γ_{xy}^2	=	coherence function
$\hat{\gamma}_{x_k r_\ell}^2(f)$	=	estimated magnitude squared coherence function
Δf	=	frquency step, $1/T_d$, Hz (11.718)
Δt	=	sampling interval, $1/r(1/48000)$, s
θ	=	angular microphone location
μ	=	radial duct mode order
σ	=	hub-tip ratio, r_a/r_b
τ	=	propagation time delay
$\Phi_m(\phi)$	=	circumferential spinning component of the pressure
ϕ	=	phase angle
ω	=	frequency in rad/s, $\omega = 2\pi f$

Subscripts

Im	=	imaginary part
i	=	running segment index
Re	=	real part
x	=	signal $x(t)$
y	=	signal $y(t)$
0	=	microphone reference location

Superscripts

*	=	complex conjugate

Presented as Paper 2581 at the 12th AIAA/CEAS Aeroacoustics Conference (27th AIAA Aeroacoustics Conference), Hyatt Regency Cambridge, Cambridge, Massachusetts, 8–10 May 2006; received 15 May 2006; revision received 1 December 2006; accepted for publication 4 December 2006.

*Aerospace Engineer, Acoustics Branch, 21000 Brookpark Road.

$+$ = clockwise rotating mode
$-$ = counterclockwise rotating mode
$\bar{}$ = ensemble average

I. Introduction

TO UNDERSTAND combustion noise measured in the far field of the PW4098 engine it is necessary to investigate and understand the pressure field in the annular combustor. The data analyzed are from a Pratt and Whitney PW4098 engine. The test was conducted as part of phase 2 of the NASA Engine Validation of Noise Reduction Concepts (EVNRC) Program. For this test two pressure transducers were mounted in the combustor and four far-field microphones were used. The coherent combustion noise seemed to have a modal pattern. Consequently, a restricted modal model was developed and tested to see if it was compatible with the available data. This work is reported herein. To be useful, the pressure field must be measured and analyzed in a manner consistent with the physics of the propagation process. A scheme that accomplishes this is discussed in this paper.

The pressure transducers failed during the test. Consequently, a sensor validation analysis was conducted [1]. Results of this study were used to select the data evaluated here. The pressure transducer signals and the far-field microphone signals are used to obtain the far-field coherent combustion noise output power and estimate the amount of coherent combustion noise that appears in the far field [2]. A method for separating correlated noise sources (core noise) and uncorrelated noise sources (jet noise) in far-field measurements of turbojet engine core noise using multiple microphones has also been developed and tested [3]. Results from the pressure transducer validation study conducted [1] and this study of annular duct modes measured in the combustor by pressure transducers are used [2,3] to interpret far-field acoustic measurements.

Combustion noise in a turbofan engine is classified according to source mechanism as either direct or indirect. Direct combustion noise is attributed to the combustion process. Indirect combustion noise is produced when hot spots pass through a turbine or nozzle. The existence of hot spots correlated with combustion noise has been shown by Miles [4]. A review of combustion and core noise is given by Mahan [5]. More recent developments are discussed by Gliebe et al. [6]. With either combustion noise source or a combination of combustion noise sources, the acoustic pressure field inside an annular combustor is governed by the solution of an eigenvalue equation. The pressure is assumed to propagate as if it were in an infinite duct. Consequently, boundary conditions at the duct ends, reflections from the duct ends, and the possibility of standing waves are not considered. The pressure propagates in particular bands identified by frequency ranges. The pressure pattern in a combustor is analyzed by breaking it up into the natural frequency bands of pressure propagation in an annular duct. Frequencies in the lowest band propagate in a plane wave mode. Higher bands move in propagating modes composed of eigenmode solutions to the annular duct eigenvalue equation governing wave propagation in an infinite annular duct with wall boundary conditions. The modes are composed of sinusoids in a circumferential direction and combinations of Bessel functions in a radial direction.

The physics of acoustic waves in hard circular ducts is discussed by Morse [7] (p. 509). The eigenvalue solution for a circular duct with flow is discussed by Eversman [8]. The physics of pressure waves propagating in annular ducts without flow is discussed by Tyler and Sofrin [9] in a treatment of axial flow compressor noise. It is also presented by Morse [7] as a problem (p. 603). Each higher mode propagates only above its own cutoff frequency. It is expected that the pressure field in a combustion duct extends over a frequency range in which several modes are propagating. The distribution of energy in the frequency band for each propagating mode is unknown and might provide insight into the physics of the propagation process. Consequently, our understanding of the pressure field in an annular combustion would be improved if one could determine the distribution of energy among duct modes.

The use of normal mode theory to analyze the propagation of noise in ducts to find the optimal microphone positions to estimate sound power from sound-pressure measurements was studied by Dyer [10]. This analysis was soon extended to look at spinning acoustic modes generated by fans [9,11–15]. This analysis has also been used to look at the modal content of noise generated by a jet in a pipe [16–19]. An acoustic modal analysis of a YF102 combustor installed in a ducted test rig was conducted by Karchmer [20] who used the assumption of equal amplitude clockwise and counterclockwise spinning modes in his analysis. Equal amplitude clockwise and counterclockwise spinning modes result in a stationary modal pattern. He found that he only needed the circumferential modes 1–6 and the corresponding zeroth order radial modes in his reconstruction of the measured data. Acoustic modal analysis of the pressure field in the tailpipe of a turbofan engine was conducted by Krejsa and Karchmer [21], and again the assumption of equal amplitude clockwise and counterclockwise spinning modes was used in the data analysis.

Before duct mode theory was applied to study core noise other techniques were used. Core noise from a Pratt and Whitney JT8D was studied by Grande [22] using multiple microphone measurements to obtain auto- and cross-power spectra in a tailpipe extension as well as far-field autopower spectra. Ten internal microphones were used to obtain measurements of narrow-band and one-third octave band pressure level spectra in an Avco Lycoming YF102 combustor by Wilson and O'Connell [23–25]. Core noise in General Electric engines has been studied by Matta et al. [26] to relate performance with emissions and noise. Coherence functions and transfer functions were used by Moore and Doyle [27] in a core noise investigation of the CF6-50 turbofan engine. They used five pressure transducers in the combustor, nine other internal sensors, and 15 far-field microphones. Moore and Doyle [27] removed the time delays between the internal and far-field signals using a cross-correlation analysis. Moore and Doyle [27] set the number of averages they used to 100 and as a consequence data below coherence function values of less than 0.1 are ignored. In this paper, the coherence function is plotted on a log amplitude scale because the coherence floor is near 0.01. Moore and Doyle [27] tried to identify the source location from vectoring of cross-correlation time delays and did not do a modal study. However, examination of internal coherence and transfer function plots indicate that combustion modes might be present. In addition, Moore and Doyle [27] do state that the appearance of a double peak with positive and negative time delays in some of the cross-correlation plots suggest that waves are moving circumferentially around the combustor.

This study was conducted to understand far-field acoustic measurements related to turbofan engine core acoustic noise as part of a noise reduction research program. However, related investigations of turbofan combustors and annular duct modes are made to understand combustion instability. A tutorial on this topic is given by Dowling and Stow [28]. An interesting three-dimensional linear acoustic analysis of gas turbine combustion instability is given by You et al. [29]. The presence of annular duct modes is also a fundamental element in the study of fan noise (Envia [30]), fan noise radiation from a turbofan engine inlet and aft ducts (Nallasamy [31]), and compressor noise (Enghardt et al. [32]).

The problem of mode propagation in an annular combustor is complex due to the presence of high speed flows and temperature gradients. The results given here are limited to using circumferential modes which resemble plane waves and the plane wave mode to replicate the measurements. To analyze the pressure distribution in a duct into its modes, it is necessary to be able to measure the relationships among the pressures at many different points. However, for this test measurements were available at only two points. Consequently, in this paper we only investigate the feasibility of using a restricted pressure modal model to replicate the single measured relationship.

The investigation discussed will

1) Show the pressure transducer instrumentation was functioning.

2) Provide evidence the peaks and dips in the measured autospectra and cross-spectra magnitudes are due to duct

propagation modes rather than a fluctuating pressure generating mechanism.

3) Identify the energy distribution in the plane wave mode.

4) Examine the validity of the assumption that one has equal amplitude clockwise and counterclockwise spinning modes.

5) Test the idea that the data can be reconstructed using the first few circumferential modes, $m = 1$, $m = 2$, $m = 3$, ..., and the corresponding zeroth order radial modes $\mu = 0$.

6) Determine the energy distribution in each band of frequencies composing a propagation mode.

This paper has two distinct aspects. Because pressure measurements were only available from two transducers, the modal decomposition methodology is restricted to two modes at a time. In addition, we must note that acoustic propagation of sound by a spinning mode of order m and frequency f will occur only if its frequency is greater than a cutoff frequency, f_{cutoff}. One natural outcome of using an appropriate number of microphones is the automatic identification of the cutoff frequencies of each mode. Consequently, a procedure to estimate the value of the cutoff frequency for each mode will be discussed.

II. Experiment

The two pressure measurements made in a Pratt and Whitney PW4098 combustor will be discussed next. The measurements were made in a study of aircraft engine core noise conducted as part of the NASA EVNRC Program. The pressure transducer at 127 deg is identified as sensor 1 and produces a pressure signal, $p_0(t)$ while the other at 337 deg is identified as sensor 2 and produces a pressure signal, $p_\theta(t)$. Sensor angles are measured clockwise from top dead center viewed from the rear. The combustion chamber is annular. The PW4000 was fitted with 24 injectors [33].

The spectral estimate parameters are shown in Table 1. The signal processing algorithms used were written in FORTRAN. They are based on subprogram modules developed by Stearns and David [34]. They were modified for this project to provide for a time delay selection. In the calculations the segments were overlapped by 50%. Results of 10 sets of data measured on the first test day are reported herein. This paper shows typical results using four sets of combustor measurements. The values of N1 CORR. used in the examples are 1622 rpm, 1750 rpm, 1900, and 2101 rpm.

A. Measurement of Autospectra and Cross Spectra

For discrete time signals the computation procedure is as follows. The total record length T_{total} for received signals $p_\theta(t)$ and $p_0(t)$ is divided into n_d disjoint (independent) data segments/blocks, each of length $T_d = T_{\text{total}}/n_d$ so that there is an ensemble of measurements $\{p_{\theta i}(t)\}$ and $\{p_{0i}(t)\}$

$$\begin{aligned} \{p_{\theta i}(t)\} &= \{s_2(t) + q_\theta(t)\}_i, \qquad i = 1, \ldots, n_d \qquad 0 \le t \le T \\ \{p_{0i}(t)\} &= \{s_1(t) + q_0(t)\}_i, \qquad i = 1, \ldots, n_d \qquad 0 \le t \le T \end{aligned} \tag{1}$$

where $q_\theta(t)$ and $q_0(t)$ are the contaminating noise at receiver location 1. Angular positions θ are relative to sensor 1 at 227 deg which was used as an arbitrary reference $\theta = 0$ deg location. The relative angular location of sensor 2 at 337 deg is then $\theta = 210$ deg.

Table 1 Spectral estimate parameters

Parameter	Value
Segment length, i.e., data points per segment, Np	4096
Sample rate, r, samples/s	48,000
Segment length, $T_d = Np/r$, s	0.08533
Sampling interval, $\Delta t = 1/r$, s	2.0833×10^{-5}
Frequency step, $\Delta f = 1/T_d$, Hz	11.718
Upper frequency limit, $f_c = 1/2\Delta t = r/2$, Hz	24,000
No. of frequencies, $Ly = f_c/\Delta f = Np/2$	2048
Time delay, $\tau = 6323/48,000$, s	0.1317
No. of independent samples	234
Overlap	0.50
Sample length, s	20

Using notation similar to that used by Piersol [35], the one-sided autospectra, $\bar{G}_{00}(f)$, $\bar{G}_{\theta\theta}(f)$ and the cross spectrum $\bar{G}_{0\theta}(f)$ are estimated for a given pair of random pressure signals, at a frequency f as

$$\bar{G}_{00}(f) = \overline{P_0(f)P_0^*(f)} = \frac{2}{T_d n_d}\sum_{i=1}^{n_d} P_{0i}^*(f)P_{0i}(f) \tag{2}$$

$$\bar{G}_{\theta\theta}(f) = \overline{P_\theta(f)P_\theta^*(f)} = \frac{2}{T_d n_d}\sum_{i=1}^{n_d} P_{\theta i}^*(f)P_{\theta i}(f) \tag{3}$$

$$\bar{G}_{0\theta}(f) = \overline{P_0(f)P_\theta^*(f)} = \frac{2}{T_d n_d}\sum_{i=1}^{n_d} P_{\theta i}^*(f)P_{0i}(f) \tag{4}$$

where the $\bar{}$ indicates an ensemble average and $P_{\theta i}^*(f)$ and $P_{0i}(f)$ are the Fourier transform of the measured pressure signals at the reference position and at the angle θ. The * designates the complex conjugate. The Fourier transforms used are windowed Fourier transforms:

$$\begin{aligned} w(\tau) = \left(1 - \frac{|\tau|}{T_d}\right) \qquad P_{\theta i}^*(f) &= \int_0^{T_d(i)} w(\tau)p_{\theta i}(\tau)e^{j2\pi f\tau}\,\mathrm{d}\tau \\ P_{0i}(f) &= \int_0^{T_d(i)} w(\tau)p_{0i}(\tau)e^{-j2\pi f\tau}\,\mathrm{d}\tau \end{aligned} \tag{5}$$

where $w(\tau)$ is a weighting function also known as a window function. This one is known as a Bartlett (triangular) window. In practice these quantities are computed using fast Fourier transforms and a nonparametric technique of spectral estimation known as periodogram averaging. Several nonparametric techniques of spectral estimation are available to be used in evaluating spectra of random data (Stearns [36], Sec. 15.6 or Hayes [37], Sec. 8.2). These techniques differ in the selection of rectangular, Bartlett, Hanning, Hamming, or Blackman window functions. In addition, the data sequences averaged may be calculated so that they overlap by varying amounts. Also, the window functions can be applied to each sequence or the whole data history. The Bartlett (triangular) window is used in discussions herein and of the aligned and unaligned coherence technique by Miles [2] because it provides a simple way to convey the idea of a window function. Issues to consider in picking a method involve consideration of statistical estimates of bias and variance and spectral resolution. The estimate $\bar{G}_{0\theta}(f)$ is a complex number such that

$$\bar{G}_{0\theta}(f) = \bar{G}_{\text{Re}}(f) - j\bar{G}_{\text{Im}}(f) = |\,\bar{G}_{0\theta}(f)\,|\, e^{-j\bar{\phi}_{0\theta}(f)} \tag{6}$$

where

$$|\,\bar{G}_{0\theta}(f)\,| = [\bar{G}_{\text{Re}}^2(f) + \bar{G}_{\text{Im}}^2(f)]^{1/2} \qquad \bar{\phi}_{0\theta}(f) = \tan^{-1}\left[\frac{\bar{G}_{\text{Im}}(f)}{\bar{G}_{\text{Re}}(f)}\right] \tag{7}$$

The signal processing algorithms used were written in FORTRAN based on subprogram modules [34] which were modified for this project to be in FORTRAN 90 form. In addition, the processing scheme was changed to permit delaying one time sequence with respect to another. For these computations, a data segment/block record length of $T_d = 4096/48,000 = 0.08533$ s was used and the number of disjoint data segments/blocks was $n_d = 234$. Consequently, total record length was $T_d n_d \approx 20$ s. The analysis was done with 50% overlap so $n_{ol} \approx 468$. Other spectral estimate parameters are shown in Table 1.

The coherence is given by

$$\gamma_{0\theta}^2(f) = \frac{|G_{0\theta}(f)|^2}{G_{00}(f)G_{\theta\theta}(f)} \tag{8}$$

The measured coherence calculated using segments overlapped by 50% is given by

$$\bar{\gamma}^{\,2}_{0\theta}(f) = \frac{|\sum_{i=1}^{n_{o\ell}} P^*_{\theta i}(f) P_{0i}(f)|^2}{\sum_{i=1}^{n_{o\ell}} |P_{0i}(f)|^2 \sum_{i=1}^{n_{o\ell}} |P_{\theta i}(f)|^2} \tag{9}$$

Given measurements from two sensors to examine, we can say a sensor is providing an incorrect signal if the signals are uncorrelated with each other or the correlation changes abruptly in some irregular fashion. A procedure developed by Miles [1] based on the concept of aligned and unaligned coherence is used to determine the validity of the signals from the pressure sensors. Miles [1] shows that by comparing a coherence function calculated using aligned and unaligned time histories one may decide if the signals from two sensors are uncorrelated or have changed in some irregular fashion. The pressure data set examined in this paper was selected using this procedure. This procedure compares the normal measured coherence $\bar{\gamma}^2_{0\theta}(f)$, called the aligned coherence, with one calculated by time delaying one signal by an amount D greater than the segment/block interval T_d. The value of D is chosen so that the two signals are not in the same segment/block interval T_d, and consequently appear to the processing procedure to be uncorrelated. For this study a value of D approximately 1.5 times the segment/block interval is used. The measured unaligned coherence $\bar{\gamma}^2_{0\theta}(f, D)$ is not zero. Even if no tones are present, the coherence of two disjoint (incoherent/independent) random noise records has a value dependent on the number of independent data segments/blocks used to calculate the coherence n_d. In [2] results were obtained from computer simulation that show good agreement with the theoretical estimate of the analytical coherence threshold

$$\gamma^2_{nn} = 1 - (1 - P)^{1/(n_d - 1)} \tag{10}$$

where we use $P = 0.95$ and $n_d = n_{o\ell}$. The coherence threshold γ^2_{nn} is discussed by Carter [38,39], Halliday et al. [40] (p. 247), and Brillinger [41] (p. 317). The coherence threshold γ^2_{nn} has a value which is greater than 95% of the values of the coherence of two independent time series calculated using n_d disjoint data segments/blocks. For the values shown in Table 1 with a 50% overlap, a total record length T_{Total} of 20 s and a resolution bandwidth B_e of 11.718 Hz, the number of data segments/blocks is $n_d = 2\Delta f T_{\text{Total}} \approx 468$. The coherence of random noise for this case is $\gamma^2_{nn} = 0.00639$. The concept of aligned and unaligned coherences is discussed in more detail in [2].

In addition, if tones are present in the time signal they will be present in all ensembles averaged and appear in the unaligned and aligned coherence. In addition to aiding the identification of persistent tones, the unaligned coherence provides a reference coherence. Small values of the aligned coherence greater than the unaligned reference coherence can be easily identified as significant because one knows what the uncorrelated coherence looks like. However, the major support it provides is in determining if a sensor is providing a useful signal. If the aligned and unaligned coherences are similar then the two sensors are uncorrelated and one sensor has failed.

B. Autospectra and Cross Spectra

For the four cases discussed, measured autospectra magnitudes and cross-spectra magnitudes and phase angles are shown in Fig. 1. Both a measured and an unwrapped phase angle are shown. Although the amplitudes of the autospectra are not remarkable, the cross-spectra amplitudes and phases are quite notable. The cross spectra have pronounced peaks and dips and the phase differences have a tendency to be nearly either 0 deg or multiples of 180 deg. These features of the cross spectra are similar to those found by Karchmer [20] in his study of YF102 combustor modes. The presence of this phase angle feature in the YF102 phase spectra is a characteristic of standing circumferential waves and it was found at all conditions tested by Karchmer.

C. Coherence

The measured aligned and unaligned coherence is shown in Fig. 2 for the four cases. The coherence functions shown have a lumpy appearance which is characteristic of the presence of a modal structure and indicates that the acoustic energy is in well-defined bands. Although many coherence values are less than 0.1 the coherence is still valid. As discussed, the aligned coherence is greater than the unaligned coherence indicating the coherence is not due to random noise. The random noise coherence value is the unaligned coherence value. In addition, the measured unaligned coherence is generally below the 95% confidence value for the analytic coherence threshold of the random noise which is $\gamma^2_{nn} = 0.00639$ and is shown as the black line in Figs. 2a–2d.

Using a statistical coherence threshold procedure discussed by Miles [1], each test point was examined for validity and sensor degradation. Initially, runs with rpm in the range of 1622–2400 were used in the modal analysis. However, eventually runs with 2304 and 2400 rpm were discarded. This left eight cases.

D. Phase Angle Standard Deviation

The coherence function is especially important because the phase angle standard deviation can be related to the coherence function. In Bendat [42] and in Piersol [35] the random error in the phase estimates due to statistical sampling is given in terms of the standard deviation of the estimated phase angle $\bar{\theta}_{0\theta}$ by

$$\sigma[\bar{\theta}_{0\theta}(f)] \approx \sin^{-1}\left\{\frac{[1 - \gamma^2_{0\theta}(f)]^{1/2}}{|\gamma_{0\theta}|\sqrt{2n_s}}\right\} \tag{11}$$

where $\sigma[\bar{\theta}_{0\theta}(f)]$ is measured in radians, and as used herein n_s is selected to be the number of segments or blocks used in the spectral calculations. For the special case where the term in curly brackets is small Eq. (11) becomes

$$\sigma[\bar{\theta}(f)] \approx \frac{[1 - \gamma^2_{0\theta}(f)]^{1/2}}{|\gamma_{0\theta}|\sqrt{2n_s}} \tag{12}$$

where for the unknown coherence $\gamma^2_{0\theta}(f)$, the estimated coherence $\bar{\gamma}^2_{0\theta}(f)$ from Eq. (9) is used. A plot of the standard deviation of the phase angle in degrees versus coherence is shown in Fig. 3 for $n_s = n_d = 234$ and $n_s = n_{o\ell} = 468$. When the coherence is greater than 0.02, Fig. 3 shows that the pressure sensor cross-spectrum phase angle standard deviation should be between 20 and 13 deg. This is accurate enough if no spinning modes are present so that the measured phase angle difference is either 0 or 180 deg.

III. Analysis

A. Annular Duct Acoustics

The annular combustor noise is analyzed in terms of a spinning pressure pattern in the gap between two rigid-walled concentric cylinders $r_b < r < r_a$. However, drawings of combustor hardware presented by Hill and Peterson [43], You et al. [29], and Dowling and Stow [28] show this theory is based on an idealized combustor. The analysis resembles the fan noise analysis of Tyler and Sofrin [9] except that the mean duct flow is included. Propagation of acoustic modes in an annular duct with no mean flow is also discussed by Converse and Hoffman [44] and Moore [15]. The mean axial velocity is included in a discussion of axial flow acoustic modes propagating in a cylinder by several researchers [11,16–18,45,46] and in an annular duct by Envia [47].

Tyler and Sofrin [9] resolved the sound field into axial propagating modes $Z(z)$, circumferential spinning modes of order m, $\Phi_m(\phi) = \cos(im\phi)$ (with m wavelengths in the circumferential dimension), and radial duct modes of order μ, $E^{(\sigma)}_{m\mu}(a^{(\sigma)}_{m\mu}\frac{r}{r_b})$ (with μ nodes or zero crossings of pressure in the radial direction).

The radial distribution of pressure in an annular duct is given by

$$R(r) = E^{(\sigma)}_{m\mu}\left(a^{(\sigma)}_{m\mu}\frac{r}{r_b}\right) = J_m\left(a^{(\sigma)}_{m\mu}\frac{r}{r_b}\right) + Q^{(\sigma)}_{m\mu}Y_m\left(a^{(\sigma)}_{m\mu}\frac{r}{r_b}\right) \tag{13}$$

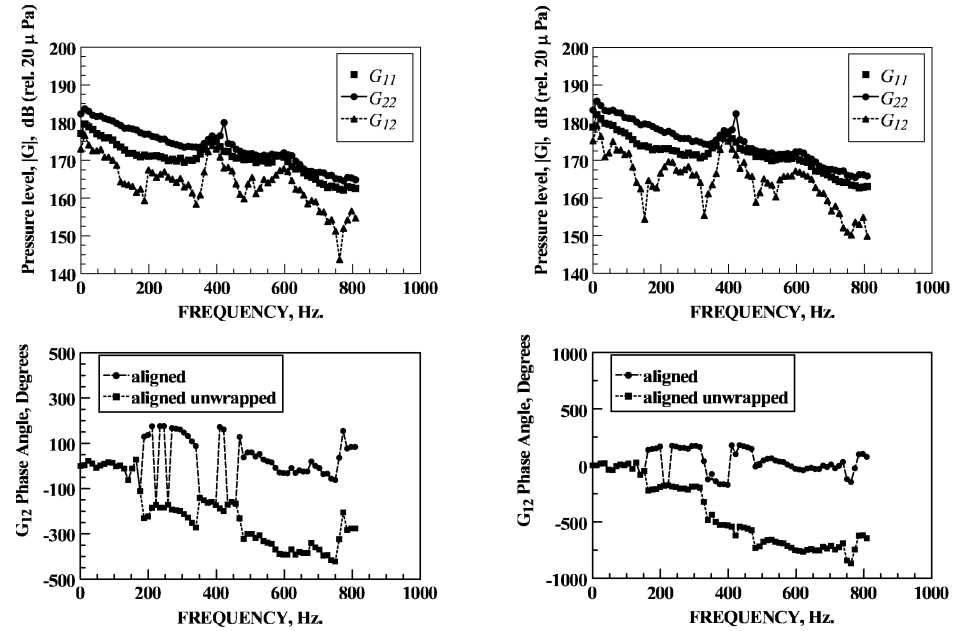

a) 1622 rpm (N1 Corr) b) 1750 rpm (N1 Corr)

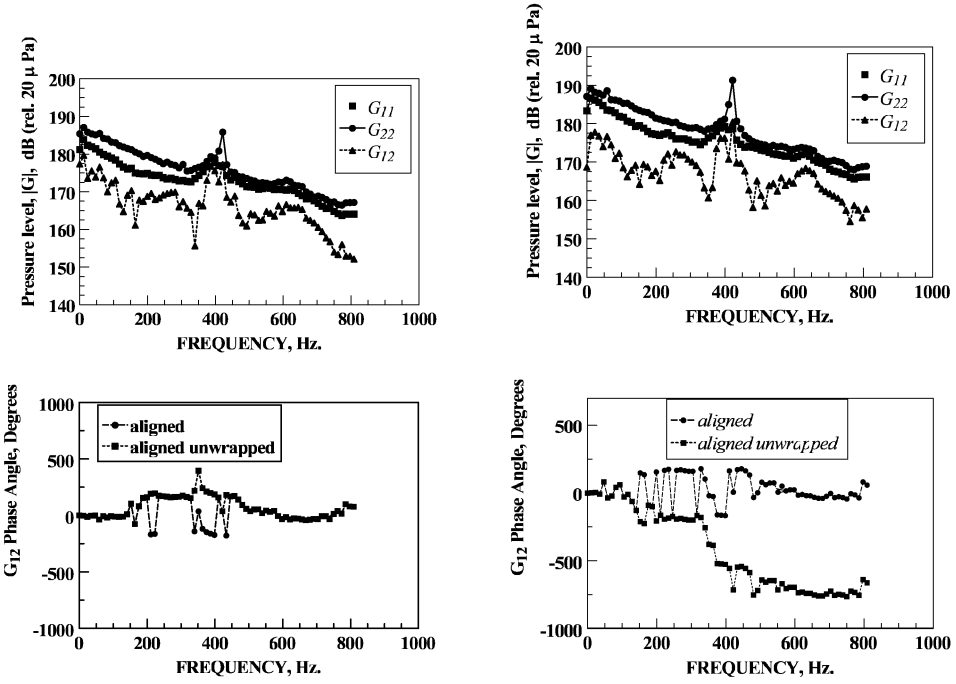

c) 1900 rpm (N1 Corr) d) 2101 rpm (N1 Corr)

Fig. 1 Autospectrum magnitude for sensor (1) at 127 deg and sensor (2) at 337 deg and cross-spectrum magnitude and phase between sensor (1) and sensor (2).

where J_m and Y_m are the Bessel functions of the first and second kind, respectively, σ is the hub-tip ratio, r_a/r_b, $a_{m\mu}^{(\sigma)}$ is the eigenvalue of the radial wave number for the (m, μ, σ) mode and it corresponds to $k_{m\mu}^{\prime(\sigma)}$ used by Tyler and Sofrin [9], $Q_{m\mu}^{(\sigma)}$ is also a function of (m, μ, σ), and r is the radius in meters. The mode shape is independent on the duct flow Mach number, M_{duct}.

The eigenvalues of the solution are given by the roots of

$$\frac{J'_m(a_{m\mu}^{(\sigma)}\sigma)}{J'_m(a_{m\mu}^{(\sigma)})} - \frac{Y'_m(a_{m\mu}^{(\sigma)}\sigma)}{Y'_m(a_{m\mu}^{(\sigma)})} = 0 \qquad r \neq 0 \tag{14}$$

where the convention that primes denote differentiation of a single argument function with respect to that argument used. Values of $Q_{m\mu}^{(\sigma)}$ can be determined from

$$Q_{m\mu}^{(\sigma)} = \frac{J'_m(a_{m\mu}^{(\sigma)})}{Y'_m(a_{m\mu}^{(\sigma)})} \tag{15}$$

The axial propagating mode is

$$Z(z) = Z_0 \exp\left\{\frac{iz}{(1-\bar{M}_{\text{duct}}^2)} \times \left\{\bar{M}_{\text{duct}} k \pm \left[k^2 - \left(1-\bar{M}_{\text{duct}}^2\right)\frac{(a_{m\mu}^{(\sigma)})^2}{r_b^2}\right]^{1/2}\right\}\right. \tag{16}$$

where $k = \omega/c$, $\omega = 2\pi f$ is the frequency in rad/s, f is the frequency in Hz, and c is the speed of sound in m/s. From Eq. (16), if k^2 is less than $(1-\bar{M}^2)[(a_{m\mu}^{(\sigma)})^2/r_b^2]$, the traveling wave solution is attenuated

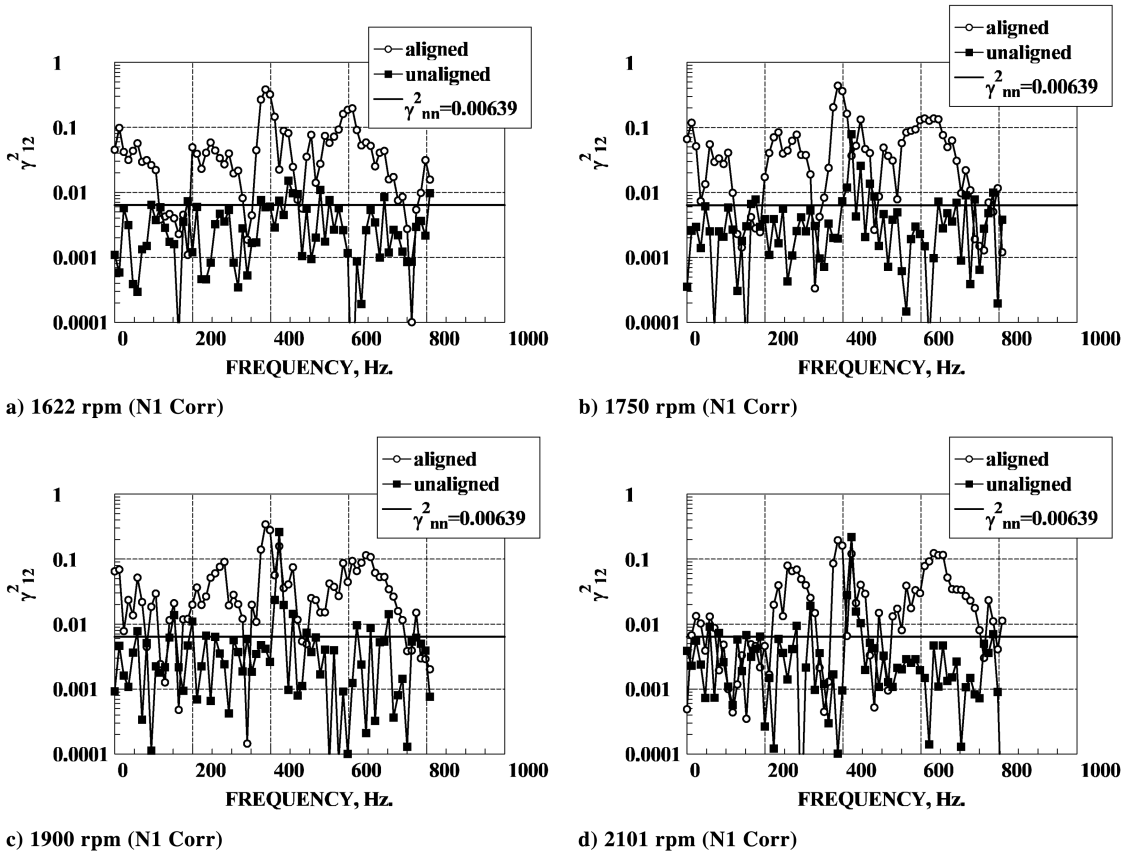

Fig. 2 Comparison of aligned and unaligned coherence between combustor sensor (1) at 127 deg and combustor sensor (2) at 337 deg.

with distance. From this relationship the frequency f of a propagating disturbance must be greater than f_{cutoff} where

$$f_{\text{critical}} = \frac{c}{2\pi}\frac{(a_{m\mu}^{(\sigma)})}{r_b} \tag{17}$$

$$f_{\text{cutoff}}(\bar{M}_{\text{duct}}) = \sqrt{(1-\bar{M}_{\text{duct}}^2)}f_{\text{critical}} \tag{18}$$

Table 2 shows the zero flow eigenvalues $(a_{m\ell}^{(\sigma)})$, $Q_{m\mu}^{(\sigma)}$, and the cutoff frequencies, $f_{\text{cutoff}} = (a_{m\mu}^{(\sigma)})c/2\pi r_b$ for the first five order modes and $\mu = 0$ using $T = 1619.37$ K, $\sigma = 0.66$, $r_a = 0.558$ m, $r_b = 0.837$ m, and $c = 806.7$ m/s. The topic of cutoff frequencies will be discussed further in Sec. III.D where the method used to select the modal span frequencies will be presented.

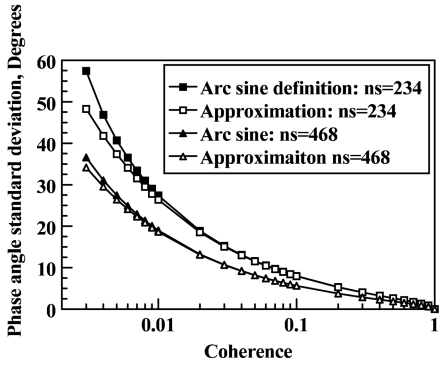

Fig. 3 Standard deviation of $G_{0\theta}$ phase angle as a function of $\gamma_{0\theta}^2$ for $n_s = 234$ and 468.

B. Modal Decomposition Method

The approach implemented here is based on the mathematical modal decomposition technique used by Karchmer [20]. The analysis starts by assuming that a randomly occurring instantaneous pressure disturbance produced by the combustion process sends a clockwise and counterclockwise pressure wave moving around the annulus. At an angle θ the two waves add to produce the resulting pressure written in terms of annular duct modes:

$$p_\theta(t) = P_\theta^+(t) + P_{\bar{\theta}}^-(t) = e^{j\omega t}\sum_{m=0}^{M-1}[A_m e^{j(\phi_m - m\theta)} + B_m e^{j(\phi_m + m\theta)}] \tag{19}$$

where A_m and B_m are the amplitudes of the clockwise and counterclockwise pressure waves associated with the lowest radial order of the mth circumferential mode, ϕ_m is the phase of the mth mode, $j = \sqrt{-1}$, and M is the total number of modes present. Note higher order radial modes are neglected. At the reference angle where $\theta = 0$

$$p_0(t) = P_0^+(t) + P_0^-(t) = e^{j\omega t}\sum_{m=0}^{M-1}[A_m + B_m]e^{j\phi_m} \tag{20}$$

Table 2 Cutoff frequencies ($T = 1619.37$ K, $r_a = 0.558$ m, $r_b = 0.837$ m, $c = 806.7$ m/s, $\bar{M}_{\text{duct}} = 0$)

Order m	Node sequence no., μ	$(a_{m\mu}^{(\sigma)})$	$f_{\text{cutoff}} = \frac{(a_{m\mu}^{(\sigma)})c}{2\pi r_b}$, Hz	$Q_{m\mu}^{(\sigma)}$
1	0	1.207637	185.245	−0.408810
2	0	2.412094	370.003	−0.348305
3	0	3.610271	553.797	−0.314771
4	0	4.799250	736.181	−0.270046
5	0	5.976450	916.757	−0.223789

Consequently, the cross spectrum $P_0P_\theta^*$ is

$$P_0P_\theta^* = \sum_{m=0}^{M-1}[A_m + B_m]e^{j\phi_m} \sum_{n=0}^{N-1}[A_n e^{-j(\phi_n - n\theta)} + B_n e^{-j(\phi_n + n\theta)}]$$
$$= \sum_{m=0}^{M-1}\sum_{n=0}^{N-1}(A_mA_n + B_mB_n)e^{j(\phi_m - \phi_n + n\theta)}$$
$$+ \sum_{m=0}^{M-1}\sum_{n=0}^{N-1}(B_mB_n + A_nB_m)e^{j(\phi_m - \phi_n - n\theta)} \quad (21)$$

After taking the ensemble average the products become correlations. The assumption is now made that the modes are independent. Consequently, the cross correlations vanish. All terms in the averaged version of Eq. (21) for which $m \neq n$ vanish.

$$\overline{P_0P_\theta^*} = \sum_{m=0}^{M-1}(\overline{A_m^2} + \overline{B_mA_m})e^{jm\theta} + \sum_{m=0}^{M-1}(\overline{B_m^2} + \overline{A_mB_m})e^{-jm\theta} \quad (22)$$

Using the definition $e^{jm\theta} = \cos(m\theta) + j\sin(m\theta)$ and noting that

$$\overline{(A_m + B_m)^2} = \overline{A_m^2} + 2\overline{B_mA_m} + \overline{B_m^2} \quad (23)$$

It follows that Eq. (22) becomes

$$\overline{P_0P_\theta^*} = \sum_{m=0}^{M-1}\overline{(A_m + B_m)^2}\cos m\theta + j\sum_{m=0}^{M-1}(\overline{A_m^2} - \overline{B_m^2})\sin m\theta$$
$$= \overline{P_0P_\theta^*}_{Re} + j\overline{P_0P_\theta^*}_{Im} = |\overline{P_0P_\theta^*}|e^{j\phi_{0\theta}} \quad (24)$$

$$|\overline{P_0P_\theta^*}| = [(\overline{P_0P_\theta^*})_{\mathrm{Re}}^2 + (\overline{P_0P_\theta^*})_{\mathrm{Im}}^2]^{1/2} \quad (25)$$

Equation (24) is the general expression for the complex cross spectrum between the pressure measured at the reference position and the pressure measured at a given angle θ relative to the reference position. The magnitude is given by Eq. (25). The phase of this cross spectrum, then, is

$$\phi_{0\theta}(A_m, B_m) = \tan^{-1}\frac{(\overline{P_0P_\theta^*})_{\mathrm{Im}}}{(\overline{P_0P_\theta^*})_{\mathrm{Re}}} = \tan^{-1}\frac{\sum_{m=0}^{M-1}(\overline{A_m^2} - \overline{B_m^2})\sin m\theta}{\sum_{m=0}^{M-1}\overline{(A_m + B_m)^2}\cos m\theta} \quad (26)$$

C. Restricted Modal Model

Equations (24) and (26), together with the single cross-spectrum measurement from the PW4098 combustor, form the basis of the modal analysis feasibility study conducted here. The approach used by Karchmer [20] assumed that only the first six modes make a significant contribution to the pressure field in the combustor over the frequency range of interest in core noise studies. Consequently, to determine six unknown values of A_m and six unknown values of B_m one would use measurements of cross-spectrum magnitude and phase at 12 positions (θ) to create 12 equations so that one could solve for 12 unknowns. However, in the study of the YF102 combustion modes Karchmer [20] found that the measured cross-spectrum phase was either 0 or 180 deg depending on the sign of the real part of the cross spectrum. Consequently, from Eq. (26) the imaginary part of the cross spectrum is zero and in evaluating modal constants A_m and B_m he could assume $A_m = B_m$. Consequently, he could then infer that the sources are such that an instantaneous pressure disturbance created in the combustor sends equal amplitude clockwise and counterclockwise pressure waves traveling circumferentially around the combustor annulus. This creates a standing circumferential pressure wave rather than a rotating or spinning circumferential pressure wave. For this case, the pressure sensor cross-spectra phase angles would have only values of 0 or 180 deg. Using this information one only needs measurements of cross-spectrum magnitude at six positions (θ) to create six equations so that one can solve for six unknown values of A_m where $A_m = B_m$. Consequently, the first assumption made is that for this case the pressure is a standing wave and $A_m = B_m$. This is done even though some of the phase angles measured seem to have intermediate values.

Table 3 Mode span

Mode, m	Low frequency, Hz	High frequency, Hz
0	0	339
1	187	550
2	339	800
3	550	800

D. Mode Span Frequencies

The theory of mode propagation and the measurements by Kerschen and Johnston indicate that modes cut on at particular frequencies [16–19]. In addition, examination of the modal decomposition of cross-spectrum spectra done by Karchmer [20] shown in Fig. 7 of his paper indicates how the cross-spectrum pattern of peaks and dips may be considered to be composed of the superposition of cut-on duct modes. The frequency range over which each mode dominates also shows up in the cross-spectrum phase angle measurements at 180 deg shown in Figs. 4(e) and 5(b) of Karchmer's paper [20]. Consequently, the second assumption made herein is that one can choose cut-on frequencies for each mode used to model the system. The cut-on frequencies were selected with annular duct acoustics theory in mind. However, the major guidance in selecting the cut-on frequencies was the measurements of coherence and cross spectra.

The effective frequency limits for each mode will be called the mode span. Examination of the modal decomposition done by Karchmer [20] shown in Fig. 7 of his paper indicates that one may easily assume that only the most recent cut-on mode is important. Consequently, in this model when mode m is cut on then the amplitude of the $m-2$ mode is set to zero. At any frequency only the amplitude of mode m and mode $m-1$ must be found. This will be designated using the notation $\sum_{m,m-1}$. Because of this restriction on the modes, the term restricted modal model is used herein.

The selected mode span frequencies are shown in Table 3 and Fig. 4. A corresponding chart of cut-on mode frequencies as a function of mode number, temperature, and Mach number is shown in Fig. 5. The cut-on mode frequencies for the $m = 1$, $m = 2$ modes are not sensitive to temperature or Mach number perturbations. At a particular temperature and Mach number many combinations of

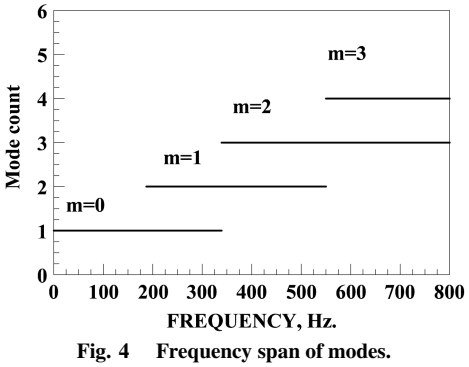

Fig. 4 Frequency span of modes.

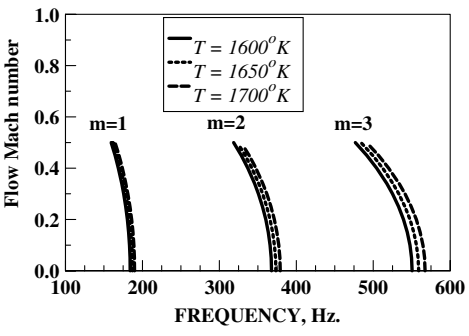

Fig. 5 Cutoff frequencies as a function of Mach number for $T = 1600$, 1650, and 1700 K.

temperatures nearby and Mach numbers nearby produce cut-on frequencies in the same general neighborhood. Because of the lack of knowledge of the exact geometry and operating conditions of the combustor, the same mode span table is used for all test conditions. Adjustments were made to the table so that the values in the table produced reasonable agreement with the theory and the measurements. The temperature range used was selected based on the combustion product mixture leaving the combustor and entering the turbine as shown in Fig. 6.22 of Hill and Peterson [43].

E. Other Assumptions and Solution Procedure

The final assumption is that the reconstructed model autospectrum $|\overline{P_0 P_0^*}|^2$ should be less than or equal to the measured autospectrum.

Using these assumptions we have a measurement of cross-spectrum magnitude and phase and two equations and two unknowns, $A_m(f)$ and $A_{m-1}(f)$, at each frequency. The two equations are written in complex notation as

$$|\bar{G}_{0\theta}(f)|e^{j\bar{\phi}_{0\theta}(f)} = |\overline{P_0 P_\theta^*}(A_m(f), A_{m-1}(f))|e^{j\bar{\phi}_{0\theta}(A_m(f), A_{m-1}(f))} \quad (27)$$

where

$$\overline{P_0 P_\theta^*(A_m(f), A_{m-1}(f))} = \sum_{m,m-1} 4\overline{A_m^2}\cos(m\theta) \quad (28)$$

$$|\overline{P_0 P_\theta^*(A_m(f), A_{m-1}(f))}|^2 = \left\{ \sum_{m,m-1} 4\overline{A_m^2}\cos(m\theta) \right\}^2 \quad (29)$$

$$\bar{\phi}_{0\theta}(f) = \overline{\phi_{0\theta}(A_m, A_{m-1})} = \begin{cases} 0 \text{ or } 360 \text{ deg}: & \overline{P_0 P_\theta^*} > 0 \\ 180 \text{ deg}: & \overline{P_0 P_\theta^*} < 0 \end{cases} \quad (30)$$

$$|\overline{P_0 P_0^*(A_m(f), A_{m-1}(f))}|^2 = \left\{ \sum_{m,m-1} 4\overline{A_m^2} \right\}^2 \quad (31)$$

where a mode m is selected to start at a particular frequency.

The assumptions made that only modes m and $m-1$ are active at a frequency, that a correct particular frequency can be selected for a mode to cut on, and that the pressure wave is stationary and not spinning are not perfectly valid. In addition, the measured cross spectrum required as input to the two equations is experimentally determined and subject to nominal experimental error and statistical uncertainties. Also, the measured autospectrum includes random noise in addition to coherent signals from propagating waves. Consequently, a solution method that provides an optimum solution in a least squares sense without derivatives was used. Algorithms for minimization without derivatives are discussed by Brent [48]. The search technique used in this study is described by Powell [49] and FORTRAN computer code is given by Shapiro [50] and Kuester [51]. The code used was a modified version of the one given by Shapiro [50] which was updated to be in a FORTRAN 90 style. The cost function used is written in terms of sound pressure level and phase angle. We have

$$L_{0\theta}(f) = 10\log_{10}(|\overline{G_{0\theta}(f)}|^2) \quad (32)$$

$$L_{xx}(f) = \min[10\log_{10}(|\overline{G_{11}(f)}|^2), 10\log_{10}(|\overline{G_{22}(f)}|^2)] \quad (33)$$

$$H_{0\theta}(m,f) = 10\log_{10}(|\overline{P_0 P_\theta^*(A_m(f), A_{m-1})}|^2) + 20\log_{10}(p_k) \quad (34)$$

$$H_{00}(m,f) = 10\log_{10}(|\overline{P_0 P_0^*(A_m(f), A_{m-1})}|^2) + 20\log_{10}(p_k) \quad (35)$$

$$\phi_{0\theta}(m,f) = \overline{\phi_{0\theta}(A_m(f), A_{m-1}(f))} \quad (36)$$

$$C1(f) = [L_{0\theta}(f) - H_{0\theta}(m,f)]^2 \quad (37)$$

$$C2(f) = \begin{cases} 0: & H_{00}(m,f) \le L_{xx}(f) \\ [L_{xx}(f) - H_{00}(m,f)]^2: & H_{00}(m,f) > L_{xx}(f) \end{cases} \quad (38)$$

$$C3(f) = \begin{cases} \min[(\bar{\phi}_{0\theta}(f) - 360)^2, (\bar{\phi}_{0\theta}(f) - 0.0)^2]: & \\ \qquad : & \text{if } \phi_{0\theta}(m,f) = 0 \\ \min[(\bar{\phi}_{0\theta}(f) - 360)^2, (\bar{\phi}_{0\theta}(f) - 0.0)^2]: & \\ \qquad : & \text{if } \phi_{0\theta}(m,f) = 360 \\ (\bar{\phi}_{0\theta}(f) - 180)^2: & \text{if } \phi_{0\theta}(m,f) = 180 \end{cases} \quad (39)$$

$$C = C1(f) + 1000C_2(f) + C_3(f) \quad (40)$$

where

$$p_k = \frac{10^{(171/20)}}{0.25}$$

and Eq. (38) defines artificial constraint $C2$ which limits the magnitude of the autospectrum calculated with the restricted modal model and insures that it is near the measured autospectrum.

IV. Results

A. Reconstruction of Measured Data

One measure of the acceptability of the modal amplitudes is how well the coefficients reconstruct the measured cross spectrum using Eqs. (28–30). Results are shown in Fig. 6. It is clear that the procedure discussed is effective in finding a set of coefficients which can construct the measured amplitude and phase spectra.

A second measure of the acceptability of the modal amplitudes is the degree the reconstructed acoustic coherent autospectrum based on the coefficients [i.e., using Eq. (31)] compares with the measured autospectrum. Results are shown in Fig. 7. The measured autospectrum contains hydrodynamic pressure fluctuations and random acoustic noise and should be larger than the reconstructed coherent autospectrum. At frequencies less than 180 Hz, where only the $m = 0$ mode exists, the results are quite good as expected. At higher frequencies the artificial constraint included in the minimization procedure is forcing the reconstructed autospectrum to be near the measured autospectrum.

B. Modal Content

To characterize the model coefficients the modes are normalized by the maximum value. The normalized coefficients are shown in Fig. 8. The mode normalization coefficients are plotted in Fig. 9. Figure 9 also shows linear curve fits to the normalization coefficients.

C. Normalized Amplitude Coefficients

The normalized coefficients for all cases were studied. A few are shown in Fig. 9 with the mode number identified. The uniformity of the plots leads to the idea that one could use the mean value of the coefficients to synthesize the cross spectra at a range of angles and shaft rotation speeds. The mean was constructed using the first eight test conditions. Values for test conditions at 2304 rpm (N1 CORR) and 2400 rpm (N1 Corr) were excluded. Mean relative coefficients are shown in Fig. 10. These mean values were used to synthesize cross spectra at various angles and operating conditions using amplitudes calculated from the linear curve fit shown in Fig. 9.

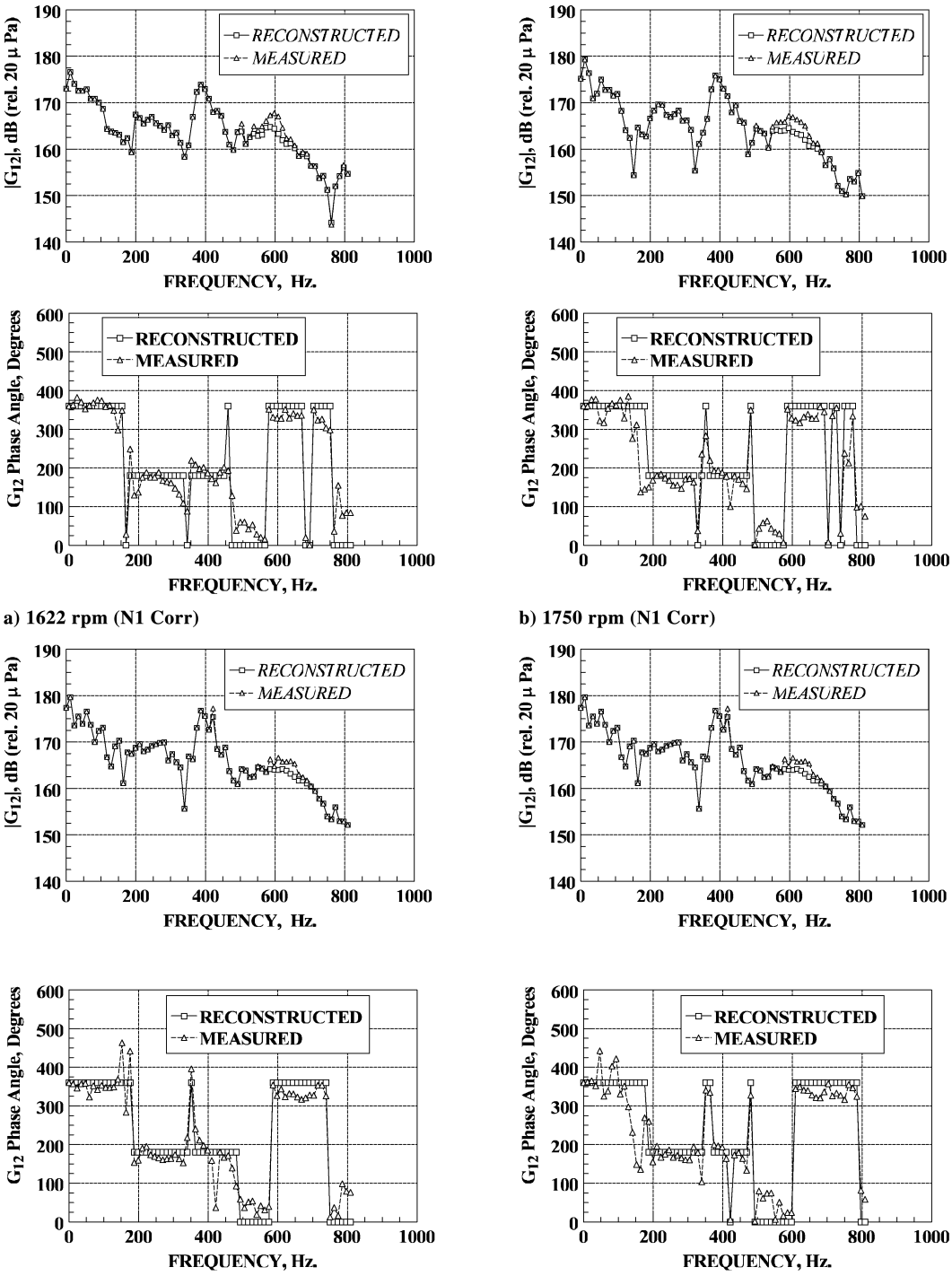

Fig. 6 Measured and reconstructed cross spectrum.

However, this paper only show comparisons with the measured data shown in Fig. 7.

V. Discussion

A treatment of the modal decomposition of the pressure field in a PW4098 engine combustor as determined by two pressure measurements was developed. A method using aligned and unaligned coherence measurements showed that the pressure transducer data presented are valid. The treatment uses the procedure of analyzing pressure propagation in the combustor in the same manner that pressure propagation in a compressor or fan is analyzed. A similar procedure was used by Karchmer [20] to analyze YF102 combustor coherence measurements made in a test stand and engine. This procedure for the operating conditions considered uses an analysis in terms of waves that propagate in modes such that for waves other than the plane wave the mode of propagation is determined by the condition that the frequency of the wave is greater than a cutoff frequency. These cutoff frequencies are determined by an acoustic eigenvalue equation, wall boundary conditions, and longitudinal boundary conditions that correspond to an infinite duct with no reflections and are given by Eqs. (17) and (18). The analysis used herein provides evidence that the peaks and dips in the measured cross-spectra magnitudes are due to annular duct acoustic propagation modes. The peaks and dips in the measured cross-spectra magnitudes are not related to

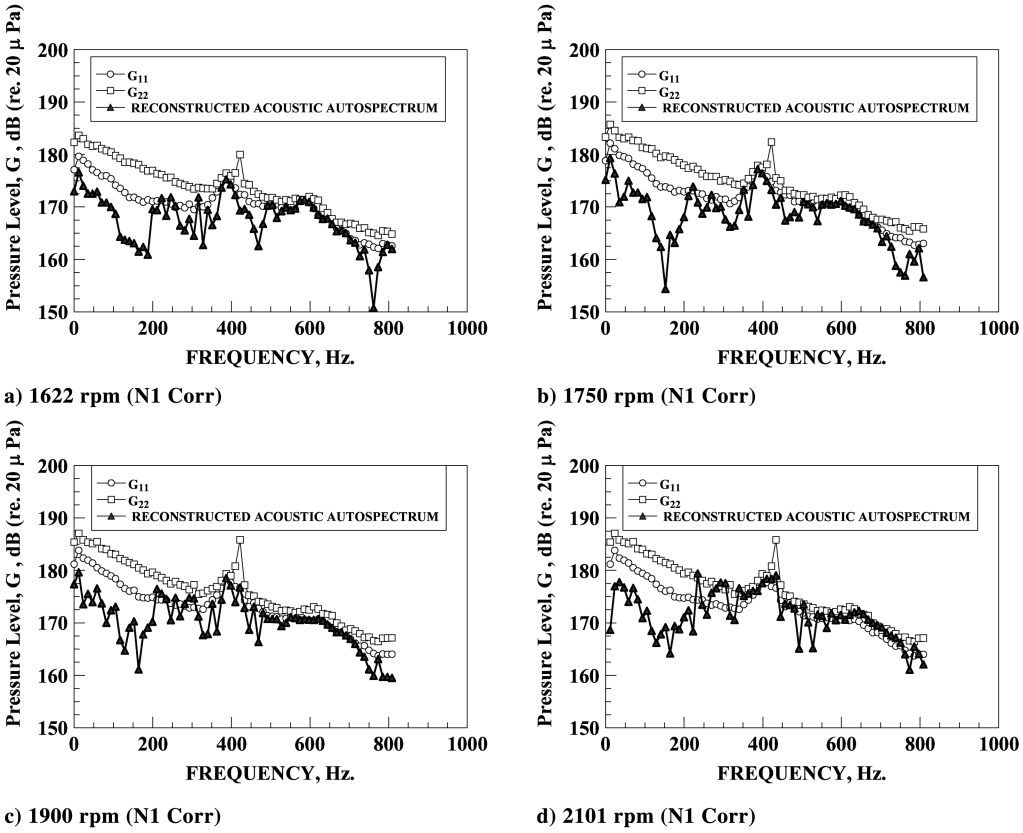

a) 1622 rpm (N1 Corr) b) 1750 rpm (N1 Corr)

c) 1900 rpm (N1 Corr) d) 2101 rpm (N1 Corr)

Fig. 7 Measured and reconstructed autospectrum.

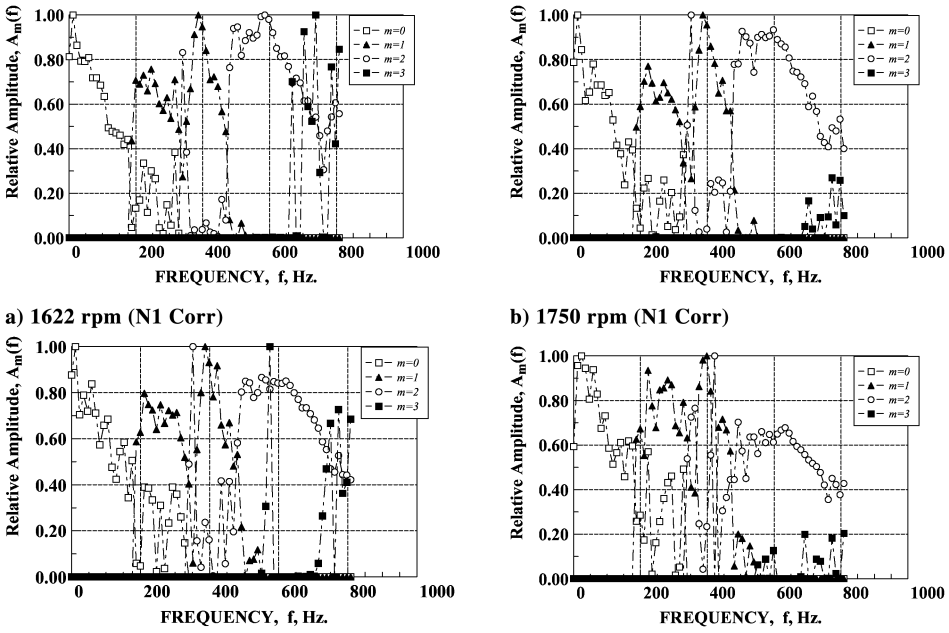

a) 1622 rpm (N1 Corr) b) 1750 rpm (N1 Corr)

c) 1900 rpm (N1 Corr) d) 2101 rpm (N1 Corr)

Fig. 8 Relative amplitudes, $A_m(f) = B_m(f)$.

longitudinal instability modes which would be at higher frequencies. The source or generating mechanism of the circumferential acoustic modes observed could be due to either direct or indirect combustion noise.

Figure 7 shows that the measured autospectra are larger than the reconstructed autospectra. This was expected because the autospectra include random hydrodynamic noise as well as correlated acoustic noise. However, Miles [2] has shown the far-field correlated combustion noise is only a small part of the total noise measured at low frequencies. In addition, Miles [2] has shown a great amount of coherent broadband noise does leave the nozzle and is observed in the far field at low frequencies. This broadband low-frequency noise may be due to indirect combustion noise generated by hot spots as they pass through the turbine as discussed by Gliebe et al. [6], pp. 209–223. However, it also might indicate that the measured autospectra in the combustor consists of

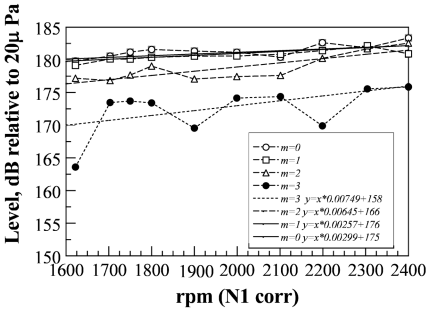

Fig. 9 Mode normalization factors and linear curve fits.

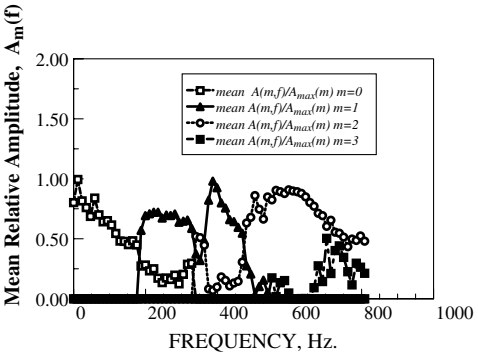

Fig. 10 Mean relative amplitudes for $m = 0$, $m = 1$, $m = 2$, and $m = 3$.

random hydrodynamic noise, broadband random acoustic noise, and correlated acoustic noise, and the acoustic noise in the far field is from the combustor. The concept that fan noise consists of tones and broadband acoustic random noise is not new and a treatment of broadband noise radiation has been given by Rice [52]. The method was also applied by Rice to the propagation of indirect combustion noise discussed in [6]. Unfortunately, the analysis of the two point measurements does not cast much light on the noise source.

The comparison of these results for the PW4098 combustor mounted in the engine with similar results for the YF102 combustor in an engine and installed in a ducted test rig [20] shows many similarities in the pressure field because the pressure field for the PW4098 and the YF102 depends on the first few circumferential modes, $m = 1$, $m = 2$, $m = 3$, ..., and the corresponding zeroth order radial modes $\mu = 0$. Because the YF102 combustor component test rig did not include any turbomachinery this fundamental structure of the pressure field seems to be independent of propagating pressure fields from either the compressor or turbine or difference tones created by interacting waves from the compressor and turbine. The fact that the energy distribution is in frequency bands with well-defined spans (see Tables 2 and 3) related to particular cutoff modes of propagation defined by Eqs. (17) and (18) explains the occurrence of well-defined bands in Fig. 2 where the aligned and unaligned coherence functions were presented.

The frequency span of the modes for this case does not resemble that in the YF102 because the PW4098 is larger than the YF102 [20]. The energy distribution in the plane wave mode and the first few circumferential modes is identified over a range of operating conditions. Because of the difference in size the energy distribution in the modes for the PW4098 is again different because the PW4098 is so much larger than the YF102 [20]. The model has two drawbacks. The first is the assumption that equal amplitude circumferential clockwise and counterclockwise pressure waves exist for each circumferential mode. The phase angles shown in Fig. 6 would be only 0, 360, or 180 deg if this were true. This assumption seems more valid for the YF102 data [20]. The second drawback is shown in Fig. 7 where the reconstructed autospectrum is far below the measured autospectrum below 200 Hz where the plane wave propagates. Above 200 Hz the difference between the measured and reconstructed autospectrum is not very large.

The successful use of the same modal span frequencies over a range of operating conditions for this particular engine suggests that the circumferential cut-on modal frequencies are in the same range at each operating condition. Consequently, the combustion noise spectrum related to the circumferential modes might not change much with the operating condition.

VI. Concluding Remarks

Turbofan engine acoustic measurements are generally made using only far-field microphones for certification to compare noise reduction technologies. With this type of instrumentation it is difficult to obtain sufficient knowledge about noise sources so that advances can be made in noise prediction and noise reduction. This paper shows that more information on combustion noise can be made available if some additional instrumentation is used.

The treatment of the modal decomposition of the pressure field in a combustor as determined by two pressure measurements developed here is in reasonable agreement with the measurements. It was applied to data from a Pratt and Whitney PW4098 engine combustor over a range of engine operating conditions. The method works well for the plane wave mode (below 200 Hz). The method gives meaningful results at higher frequencies. The method does show it is feasible to use the available measurements to produce a restricted modal model.

References

[1] Miles, J. H., "Validating Coherence Measurements Using Aligned and Unaligned Coherence Functions," AIAA Paper 2006-1389, 2006, NASA TM-2006-214113, Jan. 2006.

[2] Miles, J. H., "Aligned and Unaligned Coherence: A New Diagnostic Tool," AIAA Paper 2006-0010, 2006, NASA TM-2006-214112, Jan. 2006.

[3] Miles, J. H., "Procedure for Separating Noise Sources in Measurements of Turbofan Engine Core Noise," AIAA Paper 2006-2580, May 2006.

[4] Miles, J. H., Wasserbauer, C. A., and Krejsa, E., "Cross Spectra Between Temperature and Pressure in a Constant Area Duct Downstream of a Combustor," NASA TR TM-83351, 1983.

[5] Mahan, J. R., and Karchmer, A., "Combustion and Core Noise," *Aeroacoustics of Flight Vehicle Theory and Practice*, edited by H. H. Hubbard, NASA Reference Publication 1258, Vol. 1, Chap. 9, WRDC TR 90-3052, Aug. 1991, pp. 483–517.

[6] Gliebe, P., Mani, R., Shin, H., Mitchell, B., Ashford, G., Salamah, S., and Connell, S., "Aeroacoustic Prediction Codes," NASA TR CR-2000-210244, General Electric Aircraft Engines, 2000.

[7] Morse, P. M., and Ingard, K. U., *Theoretical Acoustics*, McGraw–Hill, New York, 1968.

[8] Eversman, W., "Theoretical Models for Duct Acoustic Propagation and Radiation," *Aeroacoustics of Flight Vehicle Theory and Practice*, edited by H. H. Hubbard, NASA Reference Publication 1258, Vol. 2, Chap. 13, WRDC TR 90-3052, Aug. 1991, pp. 101–163.

[9] Tyler, J. M., and Sofrin, T. G., "Axial Flow Compressor Noise Studies," *Transactions of the Society of Automotive Engineers*, Vol. 70, 1962, pp. 309–332.

[10] Dyer, I., "Measurement of Noise Sources in Ducts," *Journal of the Acoustical Society of America*, Vol. 30, No. 9, Sept. 1958, pp. 833–841.

[11] Mugridge, B. D., "The Measurement of Spinning Acoustic Modes Generated in an Axial Flow Fan," *Journal of Sound and Vibration*, Vol. 10, No. 2, 1969, pp. 227–246.

[12] Moore, C. J., "In-Duct Investigation of Subsonic Fan 'Rotor Alone' Noise," *Journal of the Acoustical Society of America*, Vol. 51, No. 5, 1972, pp. 1471–1482.

[13] Bolleter, U., and Crocker, M. J., "Theory and Measurement of Modal Spectra in Hard-Walled Cylindrical Ducts," *Journal of the Acoustical Society of America*, Vol. 51, No. 5, 1972, pp. 1439–1447.

[14] Harel, P., and Perulli, M., "Measurement, in a Duct, of the Space-Structure of the Discrete-Frequency Noise Generated by an Axial Compressor," *Journal of Sound and Vibration*, Vol. 23, No. 4, 1972, pp. 487–506.

[15] Moore, C. J., "Measurement of Radial and Circumferential Modes in Annular and Circular Fan Ducts," *Journal of Sound and Vibration*, Vol. 62, No. 2, 1979, pp. 235–256.

[16] Kerschen, E., and Johnston, J., "Modal Content of Noise Generated by a Coaxial Jet in a Pipe," Stanford University JIAA TR-11, N80-33177, NASA-CR-163575, Stanford University Department of Aeronautics and Astronautics, Stanford, CA, May 1978.
[17] Kerschen, E. J., and Johnston, J. P., "Modal Content of Noise Generated by a Coaxial Jet in Pipe," *Journal of Sound and Vibration*, Vol. 76, No. 1, 1981, pp. 95–115.
[18] Kerschen, E. J., and Johnston, J. P., "A Modal Separation Measurement Technique for Broadband Noise Propagation Inside Circular Ducts," *Journal of Sound and Vibration*, Vol. 76, No. 4, 1981, pp. 499–515.
[19] Kerschen, E. J., and Johnston, J. P., "Mode Selective Transfer of Energy from Sound Propagation Inside Circular Pipes to Pipe Wall Vibration," *Journal of the Acoustical Society of America*, Vol. 67, No. 6, 1980, pp. 1931–1934.
[20] Karchmer, A. M., "AcousticModal Analysis of a Full Scale Annular Combustor," AIAA Paper 83-0760, NASA TM-83334, 1983.
[21] Krejsa, E. A., and Karchmer, A. M., "Acoustic Modal Analysis of the Pressure Field in the Tailpipe of a Turbofan Engine," NASA TR TM 83387, 1983.
[22] Grande, E., "Exhaust Noise Field Generated in the JT8D Core Engine-Noise Floor Presented by the Internal Noise Sources," *Journal of the Acoustical Society of America*, Vol. 55, No. 1, Jan. 1974, pp. 30–34.
[23] Wilson, C. A., and O'Connell, J. M., "YF102 In-Duct Combustor Noise Measurements with a Turbine Nozzle-Final Report Volume 1," NASA TR CR-165562-Vol-1, LYC 81-32, N82-21031, Avco Lycoming Division, 1981.
[24] Wilson, C. A., and O'Connell, J. M., "YF102 In-Duct Combustor Noise Measurements with a Turbine Nozzle-Final Report Volume II," NASA TR CR-165562-Vol-2, N82-21032, Avco Lycoming Division, 1981.
[25] Wilson, C. A., and O'Connell, J. M., "YF102 In-Duct Combustor Noise Measurements with a Turbine Nozzle-Final Report Volume III," NASA TR CR-165562-Vol-3, N82-21033, Avco Lycoming Division, 1981.
[26] Matta, R. K., Sandusky, G. T., and Doyle, V. L., "GE Core Engine Noise Investigation Program—Low Emission Engines," FAA TR, Rept. FAA-RD-77-4, 1977.
[27] Doyle, V. L., and Moore, M. T., "Core Noise Investigation of the CF6-50 Turbofan Engine," General Electric Company, Cincinnati, OH, TR R79AEG395, Jan. 1980, NASA CR-159749.
[28] Dowling, A. P., and Stow, S. R., "Acoustic Analysis of Gas Turbine Combustors," *Journal of Propulsion and Power*, Vol. 19, No. 5, Sept.–Oct. 2003, pp. 751–764.
[29] You, D., Sun, X., and Yang, V., "A Three-Dimensional Linear Acoustic Analysis of Gas Turbine Combustion Instability," AIAA TR 2003-118, 2003.
[30] Envia, E., "A High Frequency Model of Cascade Noise," TR AIAA 1998-2318, 1998.
[31] Nallasamy, M., "Computation of Noise Radiation from Fan Inlet and Aft Ducts," *Journal of Aircraft*, Vol. 34, No. 3, May–June 1997, pp. 387–393.
[32] Enghardt, L., Tapken, U., Kornow, O., and Kennepohl, F., "Acoustic Mode Decomposition of Compressor Noise under Consideration of Radial Flow Profiles," TR AIAA 2005-2833, 2005.
[33] Gunston, B., *Jane's Aero-Engines*, Jane's Information Group, Sept. 2000, p. 514.
[34] Stearns, S. D., and David, R. A., *Signal Processing Algorithms Using Fortran and C*, PTR Prentice–Hall, Upper Saddle River, NJ, 1993.
[35] Piersol, A., "Time Delay Estimation Using Phase Data," *IEEE Transactions on Acoustics, Speech, and Signal Processing*, Vol. ASSP-29, No. 3, June 1981, pp. 471–477.
[36] Stearns, S. D., and Hush, D. R., *Digital Signal Analysis*, 2nd ed., Prentice–Hall, Upper Saddle River, NJ, 1990.
[37] Hayes, M. H., *Statistical Digital Signal Processing and Modeling*, Wiley, New York, 1996.
[38] Carter, G. C., "Receiver Operating Characteristics for a Linearly Thresholded Coherence Estimation Detector," *IEEE Transactions on Acoustics, Speech, and Signal Processing*, Vol. ASSP-25, Feb. 1977, pp. 90–92.
[39] Carter, G. C., "Coherence and Time Delay Estimation," *Proceedings of the IEEE*, Vol. 75, No. 2, Feb. 1987, pp. 236–255.
[40] Halliday, D. M., Rosenberg, J. R., Amjad, A. M., Breeze, P., Conway, B. A., and Farmer, S. F., "A Framework for the Analysis of Mixed Time Series/Point Process Data-Theory and Application to the Study of Physiological Tremor, Single Motor Unit Discharges and Electromyograms," *Progress in Biophysics and Molecular Biology*, Elsevier, New York, 1995, Vol. 64, No. 2, pp. 237–278.
[41] Brillinger, D. R., *Time Series Data Analysis and Theory*—expanded edition, Holden–Day, San Francisco, 1981, ISBN 0-8162-1150-7.
[42] Bendat, J. S., and Piersol, A. G., *Engineering Applications of Correlation and Spectral Analysis*, Wiley, New York, 1980.
[43] Hill, P. G., and Peterson, C. R., *Mechanics and Thermodynamics of Propulsion*, Addison–Wesley, Reading, MA, 1992.
[44] Converse, J. W., and Hoffman, J. D., "Acoustic Standing Waves in a Rocket Combustion Chamber with Ring and Spoke Baffles," Purde University, Jet Propulsion Center, Lafayette, IN, TR TM-67-5, N6818076, NASA CR-93262, Aug. 1967.
[45] Munjal, M. L., *Acoustics of Ducts and Mufflers*, Wiley, New York, 1987, pp. 36–38.
[46] Eversman, W., "Theoretical Models for Duct Acoustic Propagation and Radiation," *Aeroacoustics of Flight Vehicles: Theory and Practice Volume 2: Noise Control*, edited by H. H. Hubbard, NASA, Aug. 1991, pp. 101–163, Chap. 13.
[47] Envia, E., "A High Frequency Model of Cascade Noise," *Fourth Aerospace Conference*, cosponsored by the AIAA and the CEAS, NASA/TM-1998-208495, AIAA 98-2318, 2–4 June 1998.
[48] Brent, R. P., *Algorithms for Minimization Without Derivatives*, Prentice–Hall, Upper Saddle River, NJ, 1973.
[49] Powell, M. J. D., "An Efficient Method of Finding the Minimum of a Function of Several Variables Without Calculating Derivatives," *Computer Journal*, Vol. 7, No. 2, July 1964, pp. 1550–162.
[50] Shapiro, M. S., and Goldstein, M., "A Collection of Mathematical Computer Routines," New York University, TR NYU-1480-14, Feb. 1965.
[51] Kuester, J. L., and Mize, J. H., *Optimization Techniques with Fortran*, McGraw–Hill, New York, 1973.
[52] Rice, E. J., "Broadband Noise Radiation Models for Aircraft Engines," AIAA Paper 1999-1953, 1999, Addendum to *Aeroacoustic Prediction Codes*, by P. Gliebe, R. Mani, H. Shin, B. Mitchell, G. Ashford, S. Salamah, and S. Connell, NASA CR-2000-210244, 2000, pp. 229-303.

R. Lucht
Associate Editor